JMEPEG (2004) 13:335-347
DOI: 10.1361/10599490419162

1059-9495/$19.00

Superplastic Response in Al-Mg Sheet Alloys

P.A. Friedman and W.B. Copple

(Submitted 16 June 2003; in revised form 23 January 2004)

The ability to achieve large strains to failure coupled with extremely low flow stresses makes superplastic forming (SPF) an attractive option in the automotive industry for the manufacture of complex parts from aluminum (Al) sheet. However, a barrier to increased usage is the cost penalty associated with superplastic alloys, which are specially processed to have a small and stable grain size. In this article, high-temperature tensile tests are used to compare the superplastic performance of two different Al-Mg alloys that were specially processed for SPF with that of a conventionally processed Al-Mg alloy. The results of the tensile tests and optical microscopy are used to highlight the mechanisms that control deformation in each of these alloys under different test conditions. Failure in both types of materials was found to change from internal cavitation to external necking with increases in strain rate. The specially processed alloys experienced minimal grain growth or grain elongation during forming, and therefore it was assumed that deformation was controlled by grain boundary sliding. Contrary to this, the conventionally processed alloy experienced significant grain growth at the higher test temperatures, and hence it was concluded that deformation was at least partially controlled by some mechanism other than grain boundary sliding. The different deformation characteristics resulted in a different set of optimal forming conditions for the two types of materials. The SPF alloys displayed higher strains to failure at the slower strain rates and higher temperatures, while the conventionally processed alloy displayed higher strains to failure at the faster strain rates and lower temperatures.

Keywords aluminum, forming, superplastic

1. Introduction

Over the past ten years, the automotive industry has shown renewed interest in the superplasticity of aluminum (Al) alloys. This interest stems from an ongoing effort to reduce vehicle weight by replacing steel with Al in sheet metal parts. The inherent lower room temperature formability of Al compared with those of drawing-quality steels has led to significant interest in alternative forming methods, such as superplastic deformation, as ways of manufacturing complex parts from Al sheet. Superplastic forming (SPF) is usually accomplished by blow forming, in which a sheet blank is clamped in a die and gas pressure is applied to one side. This simple forming technique typically employs a single die (either male or female) rather than a matched pair, as is needed for conventional stamping. This results in a significant savings in tooling costs and can make superplastic deformation an ideal process for low-volume production. SPF has been used extensively in the aerospace sector due to limited production quantities, the need for inexpensive tooling, and the need to be able to produce complex parts from materials with relatively low formability.

While superplasticity may be a viable manufacturing option for some parts, there are limitations in the economic feasibility of this process. Superplastic response in metals is inherently coupled with microstructural aspects such as grain size, grain size stability, and resistance to cavitation. To achieve superplasticity in alloys such as Al, the sheet is usually specially processed to have a fine and stable grain size. While the extent of this special processing can range from changes in rolling schedule to compositional changes, the fact that the alloy undergoes a unique processing route typically results in an increase in material cost.

The flow stress strain-rate sensitivity of a material (i.e., the *m* value) is an indicator of its superplastic potential. This attribute, which is a function of such macroscopic forming parameters as deformation rate and temperature, is also intrinsically connected with the microstructural characteristics. As superplastic straining continues, the microstructures within these alloys tend to evolve, experiencing such phenomena as grain growth and cavity nucleation and growth. These microstructural changes often result in a loss of superplastic response, leading to premature fracture.

It is commonly believed that superplastic deformation is based on a combination of two mechanisms: diffusional creep; and thermally assisted dislocation motion. Furthermore, it is believed that the dominant deformation mechanism is a function of the imposed strain rate, the temperature, and microstructural characteristics.[1] For a thorough review of deformation mechanisms in superplastic materials see Ref. 2-4.

Superplastic materials can be produced in several different material systems that contain a fine grain structure. These materials typically have two-phase microstructures to limit grain growth, which detracts from the superplastic response. The microstructures can be divided into two basic groups: first, microduplex structures that contain roughly equal fractions of each phase; and second, quasi-single-phase materials that contain a relatively small volume of intergranular second-phase particles. The alloys of interest for the automotive industry fall within the second category. More specifically, Al-magnesium

P.A. Friedman and **W.B. Copple,** Ford Scientific Research Laboratory, Manufacturing and Processes Department, 2101 Village Road, MD 3135, Dearborn, MI 48124. Contact e-mail: pfriedma@ford.com.

(Mg) alloys, which are already used in vehicle structures, are good candidates for SPF. These alloys, containing manganese (Mn) as dispersoid formers, can be manufactured with a relatively small grain size and can show good superplastic properties.[5-7]

The requirement of a fine, stable grain structure coupled with the relatively low demand for Al-Mg alloys specially processed for SPF has resulted in a cost penalty for these materials compared with that of other Al-Mg alloys. The sensitivity of the automotive industry to material price makes it essential that this cost penalty be reduced or possibly eliminated. One method of potentially eliminating this cost is to tailor SPF processes to accommodate conventionally processed alloys or alloys that are only slightly modified. While these alloys will not exhibit the very high strains to failure that are typical in SPF, it may be possible to achieve the level of formability that is required to form most automotive panels.

In this article, a set of tensile tests that offers a relatively quick method of establishing the superplastic response of Al sheet is used to characterize two different AA5083 alloys that were specially processed for SPF as well as a conventionally processed AA5182 alloy. The results of the tensile tests coupled with optical microscopy are used both to establish the SPF potential of these alloys as well as to compare the mechanisms that control deformation in the two types of materials.

2. Material for Study

AA5083 has become the alloy of choice for automotive SPF applications due to its moderate strength, good corrosion resistance, relatively low cost, and relative ease of processing to a fine grain structure. The superplastic response of this alloy is aided by Mg, which is known to enhance recovery processes in Al alloys. Additionally, the presence of Mg, which leads to the formation of Al_6Mn precipitates, aids in minimizing strain-enhanced grain growth, which is an essential aspect of superplasticity. While 5083 (herein referred to as SPF5083) has been shown to display a modest degree of superplasticity,[5,8,9] strain hardening due to dynamic grain growth can limit the forming potential of this alloy and may lead to premature fracture.[7,10] Cavity formation can also result in premature fracture and can have deleterious effects on the post-formed mechanical properties of this alloy.[6,10]

In this article, two 5083 alloys that were specially processed for SPF are investigated from different suppliers. These alloys, labeled SPF5083-A and SPF5083-B, were both direct current-ingot cast and were rolled to final gauge. While the exact processing histories of these alloys are not available, it was reported by both manufacturers that the degree of cold roll reduction was increased compared with the process used to manufacture conventional alloys with similar composition. An alloy with similar composition but not processed for SPF was also tested under the same conditions to contrast the result with those for the superplastic alloys. The chemical compositions of both SPF alloys as well as the non-SPF, AA5182 alloy are listed in Table 1.

Table 1 Composition in wt.% of SPF5083 and AA5182 Alloys

	Temperature	Mg	Mn	Cr	Fe	Si	Al
SPF5083-A (SPF-A)	H19	4.7	0.71	0.14	0.13	0.05	Rest
SPF5083-B (SPF-B)	H19	4.6	0.75	0.11	0.19	0.07	Rest
AA5182	O	4.6	0.26	…	0.22	0.1	Rest

3. Experimental Procedures

The most efficient method of determining the mechanical response of materials at superplastic temperatures is with the elevated temperature tensile test. Due to the high sensitivity of superplastic materials to temperature coupled with the potentially large elongations, it is important that the temperature throughout the sample be accurately controlled. Additionally, the *m* value of these materials requires the use of a system with good control of deformation speed. This becomes more difficult at the very slow strain rates at which it is necessary to have a method of elongating the material at a constant rate.

3.1 Experimental Setup

Tensile tests were conducted in a MTS Sintech machine (MTS Systems Corporation, Eden Prairie, MN) with a three-zone split-furnace wrapped around specimen and pull rods. Specimen temperature was monitored on both ends of the gauge length with attached thermocouples and was maintained to within ±2 °C of the test temperature. The load frame used an 8.9 kN (2000 lb) load cell and was controlled by MTS Systems software. Tensile grips were manufactured from Inconel, a nickel-based super-alloy that is suitable for high-temperature applications. The tensile grips, shown with a sample in Fig. 1(a), are designed to push on specimen shoulders (Fig. 1b) in opposite directions while squeezing the specimen grip ends with blocks in an effort to contain the grip material. The added benefit of these blocks is somewhat limited due to creep relaxation of the grip load at the relatively high-test temperatures. It has been shown that this type of design results in straining in grip regions, thus altering the desired strain rate condition.[11] While control of strain rate is difficult, this technique offers a consistent method of characterizing superplastic sheet material.

3.2 Experimental Method

An important element in characterizing a superplastic material is determining the *m* value at different temperatures and strain rates. In this work, a single test has been developed that offers information on both the overall formability of the alloy as well as the *m* value under a specific set of experimental conditions.

Crosshead speeds (CHSs) were determined based on desired initial strain-rates and the assumption that uniform straining was occurring in the gauge length region. The flow stress dependence on the strain rate was analyzed via a jump in strain rate at a prescribed strain level. At 5% engineering strain, the

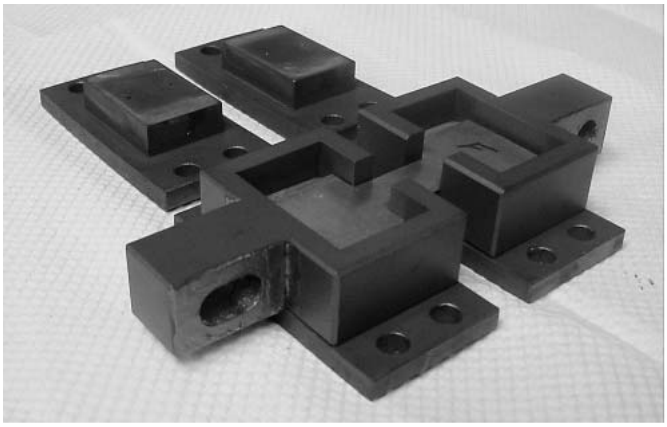

(a)

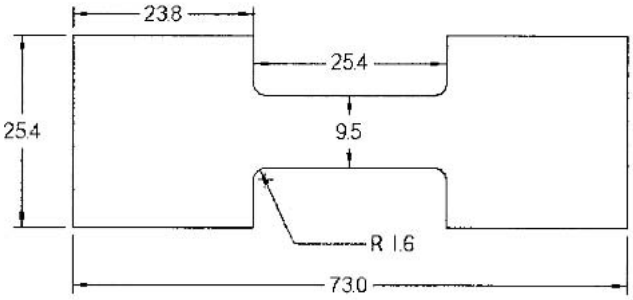

(b)

Fig. 1 (**a**) Superplastic grips made from Inconel shown with sample and face plates and (**b**) schematic of superplastic tensile specimen (dimensions in mm)

initial strain rate was doubled so that the change in flow stress could be recorded. The new CHS was based on the initial gauge length but was corrected for the 5% increase in effective gauge length. The *m* value, the *m* value, is calculated based on the increase in load due to the jump in strain rate according to:

$$m = \left(\frac{\log(P_2 / P_1)}{\log(\dot{\varepsilon}_2 / \dot{\varepsilon}_1)} \right) \quad \text{(Eq 1)}$$

where P_1 and P_2 are the flow stresses and $\dot{\varepsilon}_1$ and $\dot{\varepsilon}_2$ are the corresponding instantaneous strain rates before and after the applied jump in strain rate, respectively.

3.3 Test Matrix

To fully characterize the SPF response of these alloys, a set of tensile tests has been developed that offers a comprehensive evaluation of the material. The two measurements of interest are the *m* value (the *m* value) and total elongation. Table 2 is a list of the required tensile tests used to complete the characterization. The tests are conducted over 3 decades of initial strain rate from 1×10^{-4} s^{-1} to 1×10^{-2} s^{-1}, which encompass the band of potential strain rates that can practically be used in the SPF of most typical Al-Mg alloys. These strain rates translate to reaching an engineering strain of 50% in 67.6 min, 6.76 min, and 40.5 s, respectively. While a time of 67.6 min is impractical in production, it offers information on the low flow stress behavior of the material in which diffusional mechanisms are dominant. The fastest strain rate achieves 50% engineering strain in less than 1 min and is significantly faster than most commercial SPF processes. As in the case of the very slow test, this process may be outside the band of practical strain rates. However, it can offer important information at high flow stresses in which thermally assisted glide-climb mechanisms dominate.

Another key element in superplastic deformation is temperature. The high temperature of 525 °C is an ideal temperature for SPF of these materials.[10] However, this temperature may be difficult to use in production due to handling issues related to the very low flow stress in the material at this temperature. The lower temperature of 475 °C represents a more practical temperature for production SPF. Last, tests are performed in both the L orientation (rolling direction parallel to the tensile axis) and the T orientation (rolling direction perpendicular to the tensile axis) to gain information on planar anisotropy. SPF typically involves deformation in all planar directions, and, therefore, it is important to identify any significant differences in flow characteristics. In an effort to minimize the test matrix, a full-factorial matrix is not used, and the effect of orientation with respect to temperature is not investigated. In Table 3, the initial strain rates in the first and second stages of forming are shown with the corresponding CHSs. The gauge length is adjusted for the 5% extension in the calculation of the second-stage CHS.

Table 2 Matrix of Superplastic Tensile Tests

Specification No.	Orientation	Temperature, °C	Initial Strain Rate, 1/S	
			1	2
a	L	525	1.0×10^{-4}	2.0×10^{-4}
b	L	525	1.0×10^{-3}	2.0×10^{-3}
c	L	525	1.0×10^{-2}	2.0×10^{-2}
d	T	525	1.0×10^{-4}	2.0×10^{-4}
e	T	525	1.0×10^{-3}	2.0×10^{-3}
f	T	525	1.0×10^{-2}	2.0×10^{-2}
g	L	475	1.0×10^{-4}	2.0×10^{-4}
h	L	475	1.0×10^{-3}	2.0×10^{-3}
i	L	475	1.0×10^{-2}	2.0×10^{-2}

4. Results

4.1 Mechanical Behavior

Load versus extension data were transposed to true strain-true stress for analysis based on the assumption of uniform straining within the gauge section. Although the diffuse neck that occurs during superplastic tensile testing slightly violates this assumption, the calculated strain is used to compare the

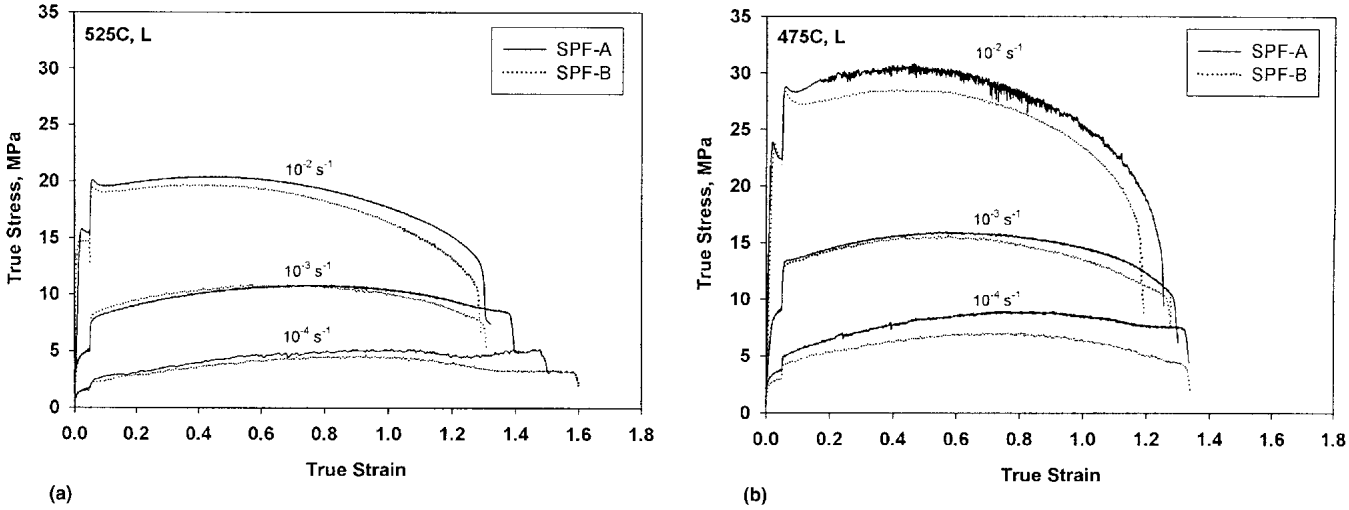

Fig. 2 True stress-true strain as determined by tensile testing for both SPF5083 alloys at 3 decades of initial strain rate at (**a**) 525 °C and (**b**) 475 °C

Table 3 Initial Strain Rates and Corresponding CHSs Used in Tensile Tests

Initial Strain Rate, 1/S		CHS, mm/s	
1	2	1	2
1.0×10^{-4}	2.0×10^{-4}	0.00222	0.00466
1.0×10^{-3}	2.0×10^{-3}	0.02220	0.04662
1.0×10^{-2}	2.0×10^{-2}	0.22200	0.46620

flow behavior of the test alloys. The true stress-true strain curves for both the SPF-A and SPF-B materials in the L orientation are shown in Fig. 2. Figure 2(a) shows the flow stress for samples deformed at three different initial strain rates at 525 °C. Flow stress for samples deformed under the same three conditions but at a lower temperature of 475 °C are shown in Fig. 2(b). All of the curves show a rapid increase in flow stress at approximately 5% strain. This correlates with the jump in strain rate used to measure the *m* value of the material. In the high strain-rate tests, there is a slight drop in flow stress immediately before the strain-rate jump. This is due to an inertial effect in the load frame as it shifts into the higher speed. This effect has been ignored in the calculations of *m* value by using the flow stress value just prior to the sudden drop in stress. For both materials, the flow stress appears to be highly correlated with strain rate, with the faster rates showing significantly higher flow stresses. Additionally, the hardening rate also appears to be a function of strain rate. The tests performed under the fastest conditions show very little increase in flow stress with increasing strain. On the other hand, there is a modest degree of hardening in the slowest test. It should be noted that after the jump in strain rate at 5% strain, these tests were performed under constant CHS conditions. With the dramatic increase in gauge length, this translates to an actual decrease in strain rate throughout the test. Based on this fact, and coupled with the positive relationship between flow stress and strain rate, these tests significantly underestimate the actual degree of material hardening that would occur under constant strain-rate conditions.

The effect of temperature on the flow behavior of these alloys can be seen by comparing the curves in Fig. 2(a) to corresponding curves in Fig. 2(b). While the shapes of the curves are similar at the two different temperatures, the maximum flow stress values at the lower temperature are on the order of 50-60% higher than those of the corresponding tests at the higher temperatures. While this result is not surprising based on the fact that the deformation mechanisms are thermally assisted, the degree of sensitivity is significant.

4.2 Total Elongation

The total elongation of test samples is used as a measure of the formability of the material, and is typically a function of strain rate, temperature, and tensile orientation. The total elongation for test alloys at 525 °C is plotted as a function of log (initial) strain rate and is shown in Fig. 3(a). Elongation appears to be correlated with strain rate, with the samples deformed at the slower rates showing larger elongations. The effect of orientation can also be identified. It appears that samples with the tensile direction parallel to the rolling direction (i.e., the L orientation) consistently achieve higher elongations than samples with the tensile direction perpendicular to the rolling direction (i.e., the T orientation). This has been reported in other superplastic Al sheet alloys and may be a result of the preferential alignment of particles along grain boundaries during the rolling process.[10]

The effect of temperature on the total elongation is shown in Fig. 3(b). Not surprisingly, the total elongation decreases at the lower temperature. However, it appears that the decrease in elongation is significantly larger for the SPF-A material at the fastest strain rate. This is possibly due to an increase in the rate of cavitation in this alloy at this temperature and strain rate.

4.3 *m* value

The *m* values as determined by Eq 1 at 5% elongation are plotted in Fig. 4(a) as a function of log strain rate for the two test alloys at 525 °C. The deformation at the relatively slow

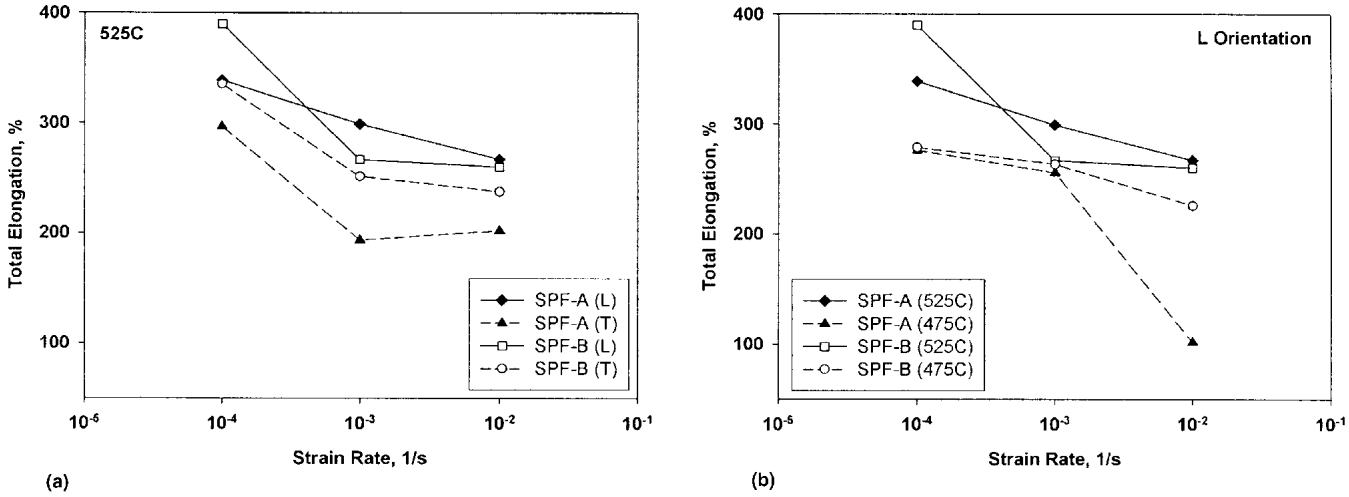

Fig. 3 Total elongation for SPF 5083 alloys plotted as a function of log initial strain rate for samples tested (**a**) at 525 °C and (**b**) in the longitudinal orientation

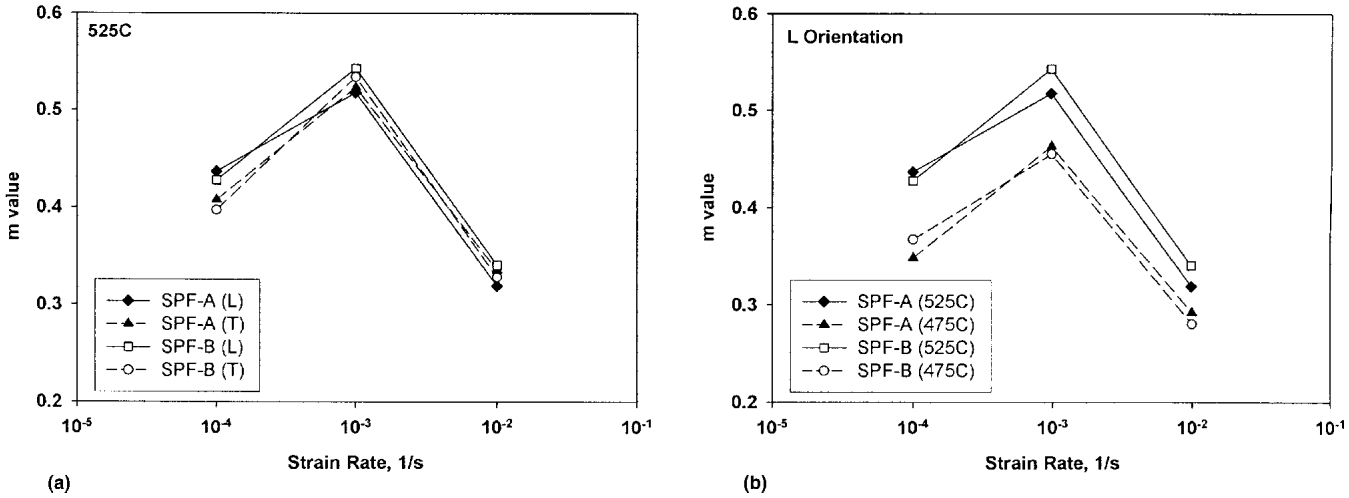

Fig. 4 The *m* values for SPF 5083 alloys plotted as a function of log strain rate for samples tested (**a**) at 525 °C and (**b**) in the longitudinal orientation

strain rate is assumed to be controlled by diffusional accommodation at grain boundaries, while the deformation at the relatively high strain rate is controlled by thermally assisted dislocation motion. At the middle strain rate, the *m* value peaks where it is assumed that both of these mechanisms are at work. The effect of orientation on *m* value appears to be small and within the margin of error for both alloys.

The effect of temperature on *m* value is shown in Fig. 4(b), where data from samples deformed in the L orientation at both 475 °C and 525 °C are shown. The *m* values of the test alloys are significantly lower at 475 °C. It is interesting to note that the general trends in the data are the same at both the high and low temperatures. Additional data will help to determine the degree of shift in maximum *m* value with temperature.

While the data presented above represent the *m* value at 5% elongation for all of the samples, it is interesting to look at the *m* value of the material as a function of strain. To accomplish this, the flow stresses for each sample at 10% strain increments were extracted from the flow data. These values were used with Eq 1 to solve for the *m* value at each 10% increment. Two sets of data were used to produce the *m* values. Flow stress data from samples deformed at the slowest rate and the middle rate were used, as well as data from the medium rate and fastest rate. These data are plotted in Fig. 5 for both of the test alloys.

The two alloys appear to behave similarly with the *m* value decreasing with strain. It is believed that this decrease is a result of a combination of grain growth and damage accumulation in the form of cavity nucleation and growth. The data taken from both alloys deformed at the 1×10^{-4} s^{-1} and 1×10^{-3} s^{-1} strain rates show significantly higher *m* values than do the data taken from samples deformed at 1×10^{-3} s^{-1} and 1×10^{-2} s^{-1} strain rates. This is consistent with the data shown in Fig. 4, where the *m* values at the lower strain rates were higher than those of the faster strain rates.

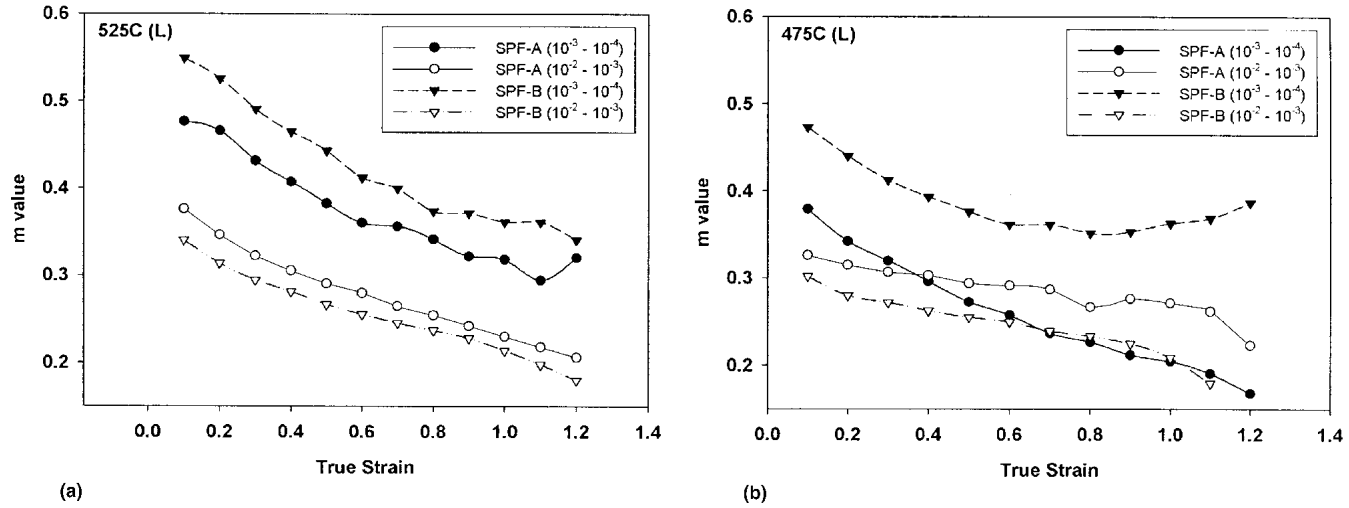

Fig. 5 The *m* value as a function of true strain for samples deformed in the longitudinal orientation at (**a**) 525 °C and (**b**) 475 °C

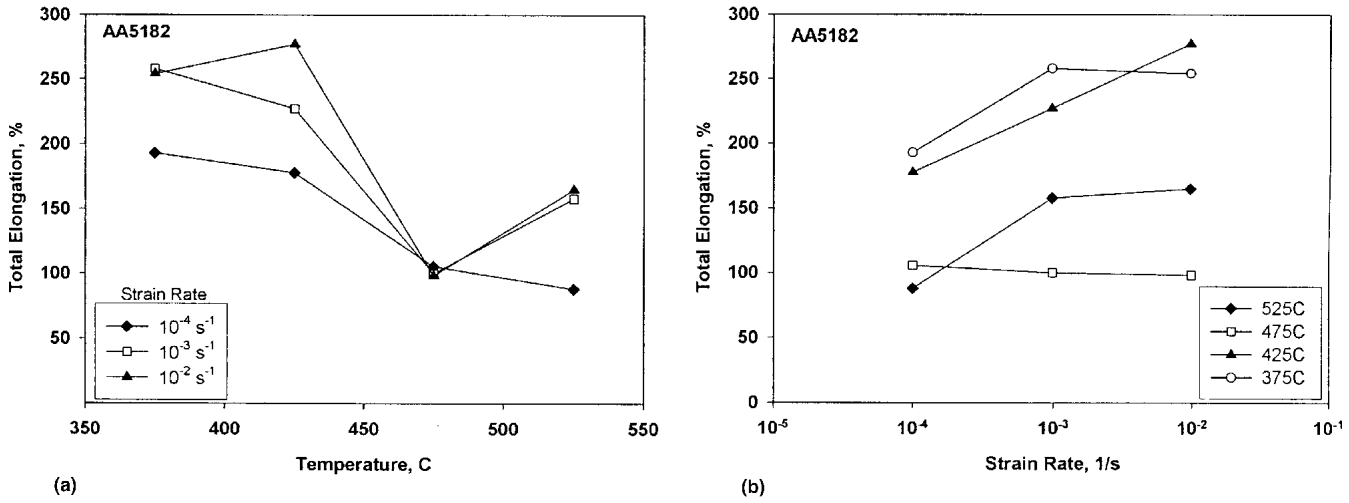

Fig. 6 Total elongation for the AA5182 alloy in the longitudinal orientation as determined by tensile testing plotted as a function of (**a**) temperature and (**b**) initial strain rate

4.4 Superplastic Response in AA5182

The test matrix listed in Table 2 was also performed on the conventionally processed AA5182 alloy. This alloy has a similar composition to the SPF5083 alloys tested except for the lower Mn level and the absence of chromium. Both of these elements help to slow grain growth at elevated temperatures.

Tests were first performed at 525 °C and 475 °C, which is similar to those of the SPF5083 alloys. However, after noting a significant dropoff in superplastic response at 475 °C the testing was expanded to 425 °C and 375 °C. Total elongation values for the AA5182 alloy in the longitudinal orientation are plotted in Fig. 6(a) as a function of test temperature for the three different initial strain rates. The trend in these data is opposite to that of the SPF5083 alloys with total elongation greatest at the lower temperatures, except for the data obtained at 475 °C. At the slowest initial strain rate of 1×10^{-4} s^{-1}, the total elongation increases steadily as the temperature is lowered. This is similar to the response at the fastest strain rate, except that at the low temperature of 375 °C there appears to be a drop in the superplastic response. Also worth noting is the similar poor superplastic response at 475 °C for all strain rates. The reason for this stems from the abnormal grain growth in this alloy at that temperature, which is discussed in detail in the next section.

The same total elongation data are plotted in Fig. 6(b) as a function of initial strain rate for four test temperatures. The data indicate that the superplastic response of this alloy generally increases for faster strain rates, except for the data at 475 °C. This is the exact opposite trend to that of the SPF5083 alloys. This difference is most likely due to faster grain growth kinetics in the AA5182 alloy compared with those in the SPF alloys and to the long forming times associated with the lower strain rates (see below). That is, the AA5182 alloy loses superplastic potential with time faster than does either of the SPF alloys.

The *m* value of the AA5182 alloy plotted as a function of strain rate for four test temperatures is shown in Fig. 7. While the SPF alloys display a strain rate-*m* value relationship that is similar to those of the SPF5083 alloys, the AA5182 alloy shows the highest *m* value at the slow strain rate of 1×10^{-4} s^{-1} and decreases at faster strain rates. As mentioned earlier, the strain rate for the peak *m* value will shift to slower strain rates for materials with coarser grains. It is possible that the strain rate for peak the *m* value in this alloy is less than 1×10^{-4} s^{-1}. It is worth noting that the highest total elongations were attained under test conditions that produced the lowest *m* value.

4.5 Microscopy

Samples for microscopy were quenched immediately after testing to capture the microstructure at the time the test was completed. The specimens were then aged for 20 h at 130 °C to highlight the microstructure. Although SPF5083 is not considered to be an age-hardenable alloy, it has been found that aging decorates grain boundaries with second-phase particles that help to reveal the microstructure. This treatment has been found to have a negligible effect on grain size.[10] Metallographic samples were prepared by mechanically polishing and etching with Graf Sergeant reagent (15.5 ml HNO_3, 0.5 ml HF, 3 g Cr_2O_3, and 84 ml water). All of the metallographic sections are shown in the L-S orientation (rolling direction parallel to the horizontal, thickness parallel to the vertical) in this article.

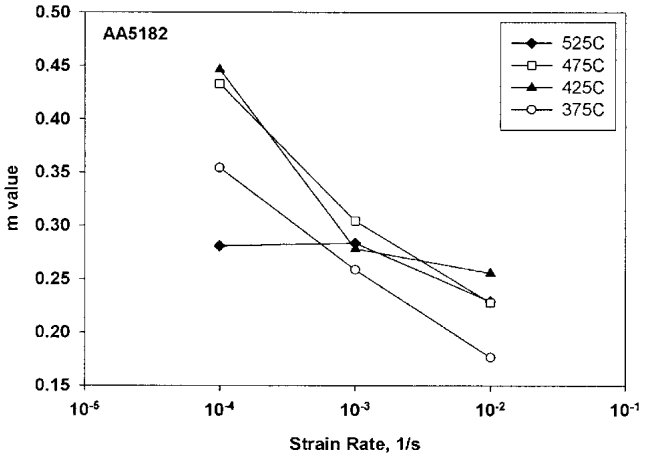

Fig. 7 The *m* value for AA5182 alloys as determined by tensile testing on samples in the longitudinal orientation

4.5.1 SPF5083 Alloy. Micrographs of the two SPF5083 alloys in the as-received H19 condition are shown in Fig. 8. While both of these alloys were received in the hardened condition (H19), the initial heating time prior to superplastic deformation causes recrystallization and the formation of an equiaxed grain structure. Sections from the grip region of the SPF5083 samples were investigated to understand the effect of the extended heat treatment on the grain structure. Since these samples were taken outside of the deformation zone, the effect of the heat treatment on the microstructure has been isolated from that of the superplastic deformation. Microstructures from grip regions of both the SPF alloys deformed at two different strain rates are shown in Fig. 9 and 10. The grains appear to be somewhat coarser in the samples deformed at the slower rate for both alloys. This is consistent with the notion that a longer forming time and, hence, a longer exposure to elevated temperature result in more grain growth.

Failure in these types of alloys is often from internal cavitation in which voids initiate at grain boundary heterogeneities such as dispersoid particles and triple points. With further deformation, these cavities grow and coalesce until failure when the material is no longer capable of withstanding the flow stress. Due to the relatively high *m* value, and therefore to the inherent resistance to necking in these alloys, it is possible for these materials to sustain a large degree of cavitation before fracture. Examples of cavitation are shown in Fig. 11, where sections of the gauge length, approximately 7 mm from the failure site of material SPF-A, at three different strain rates are shown. The cavities have a jagged appearance as a result of their intergranular nature. Additionally, there appears to be a large effect of strain rate on the amount of cavitation, with the

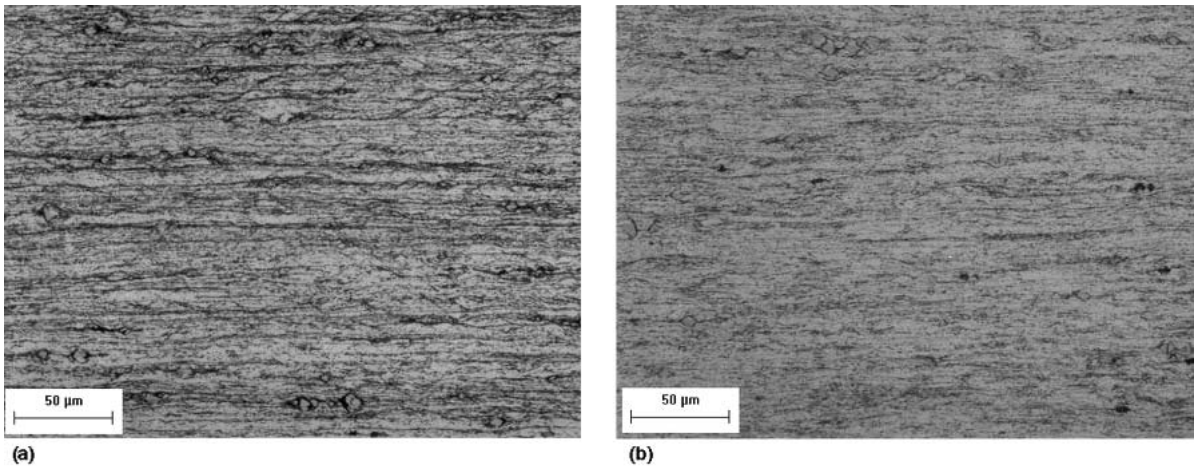

Fig. 8 Micrographs of the as-received (**a**) SPF-A alloy and (**b**) SPF-B alloy. Rolling direction is shown in the horizontal.

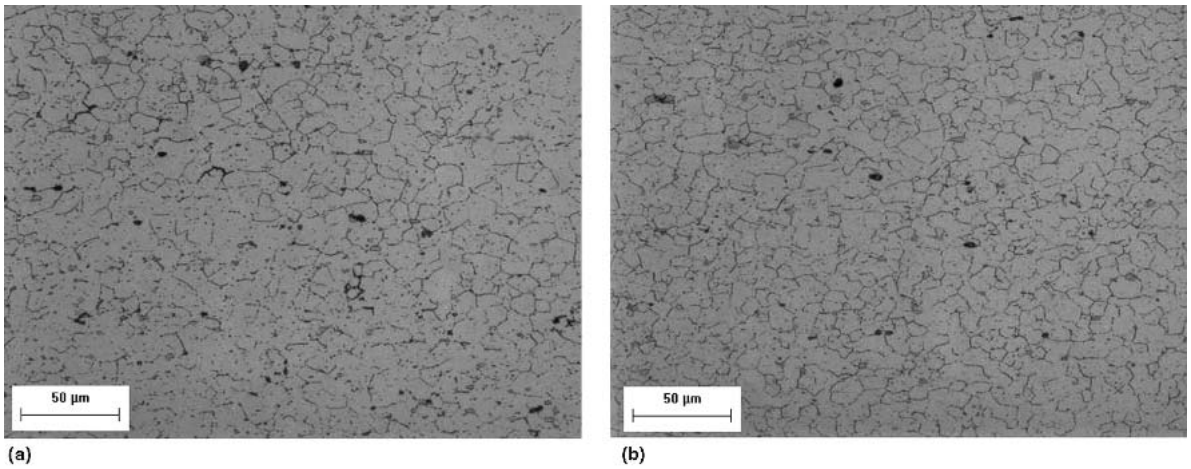

Fig. 9 Micrographs of the grip region in material SPF-A after tensile testing at 525 °C and initial strain rates of (**a**) 1×10^{-4} s^{-1} and (**b**) 1×10^{-2} s^{-1}

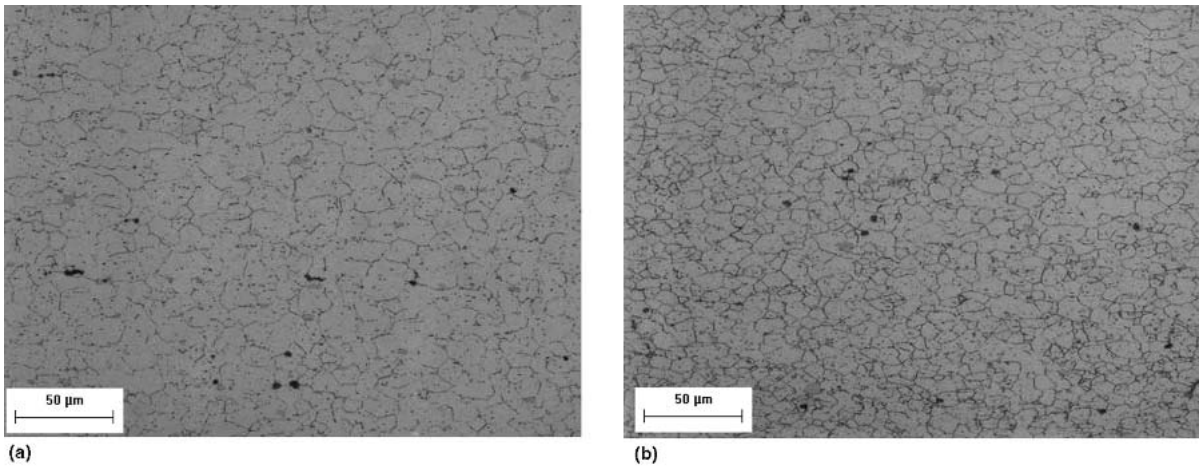

Fig. 10 Micrographs of the grip region in material SPF-B after tensile testing at 525 °C and initial strain rates of (**a**) 1×10^{-4} s^{-1} and (**b**) 1×10^{-2} s^{-1}

slower rate showing significantly more cavitation than that of the faster strain rate.

The percent cavitation was measured in these alloys by measuring the cavity area percentage of a 25 mm section of material from the gauge length. Twenty digital images of the through-thickness, similar to those in Fig. 11, were recorded at ×100 magnification along the specimen length for each specimen. Cavitation area fraction was measured with computer software for each of the 20 pictures. An average value for cavitation was recorded for each specimen, representing the degree of cavitation to occur within the most highly strained 25 mm section of the sample. These data are plotted in Fig. 12. Cavitation in both alloys appears to be correlated with strain rate, with slower strain rates having significantly higher cavitation area percentages. Test temperature appears to influence cavitation with a larger effect in alloy SPF-B than in alloy SPF-A. While these data show a different effect of test temperature, further work is required to remove the effect of varying strain levels.

4.5.2 AA5182 Alloy. A micrograph depicting the as-received microstructure of the conventionally processed AA5182-O alloy is shown in Fig. 13. The fully annealed (O temper) sample has a completely equiaxed grain structure. It is interesting to note that the grain size in the as-received AA5182 alloy is on the order of the grain size in the post-superplastically formed SPF5083 alloys.

The reverse trends in elongation and m value between the SPF5083 alloys and those of the conventionally processed alloy were investigated by looking at the microstructure of both grip and gauge regions of the AA5182 alloy samples. The material examined in the gauge region experienced an approximate 50% reduction in cross-sectional area during superplastic deformation. Micrographs from both regions for samples deformed at 1×10^{-2} s^{-1} and 1×10^{-3} s^{-1}, respectively, at 525 °C are shown in Fig. 14 and 15. The increase in grain growth caused by the longer cycle times is evident by comparing the microstructure in Fig. 14(a) to that in 15(a). Similar to the SPF alloys, the longer forming time resulted in more grain growth. It is interesting to note that the microstructure contains a wide range of grain sizes. This is most likely a result of the coarser grains growing at the expense of the adjacent finer grains, while new, smaller grains continually form due to recrystallization.

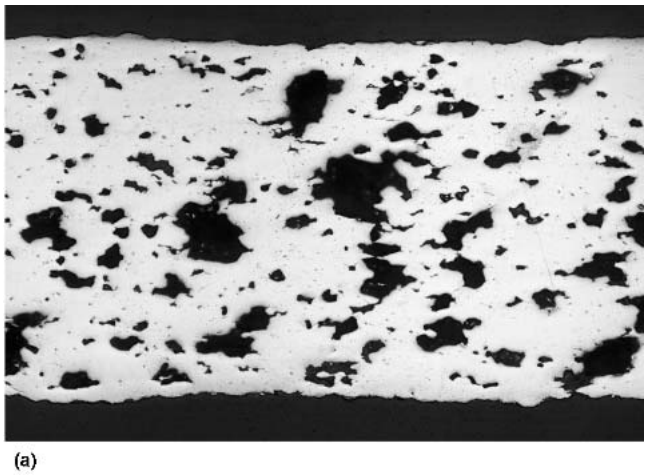

(a)

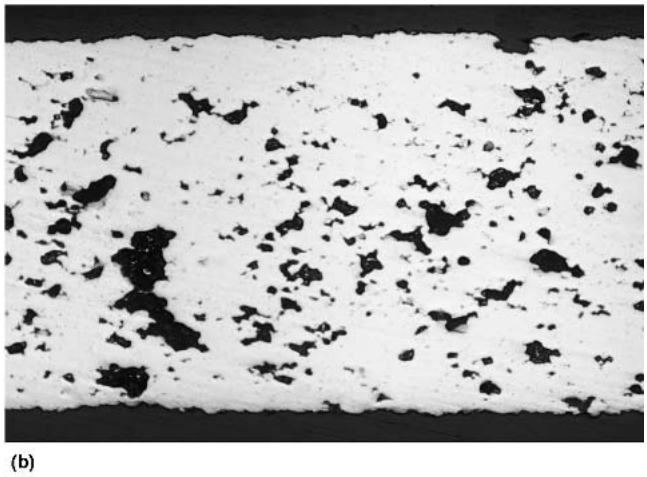

(b)

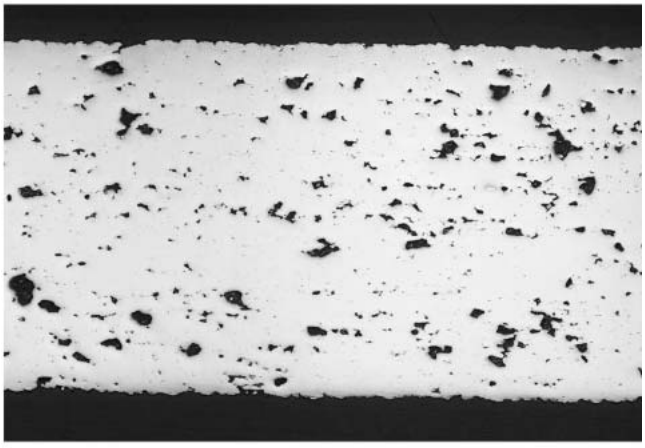

(c)

Fig. 11 Digital micrographs of the gauge section of alloy SPF5083-A showing cavitation from samples tested at 525 °C at initial strain rates of (**a**) 1×10^{-4} s^{-1}, (**b**) 1×10^{-3} s^{-1}, and (**c**) 1×10^{-2} s^{-1}. All three samples were taken from sections of the gauge length approximately 7 mm away from the failure site.

The loss of superplastic response in this alloy at the slower speed is a result of the different rate of cavitation with strain in the samples deformed at the two different strain rates. The

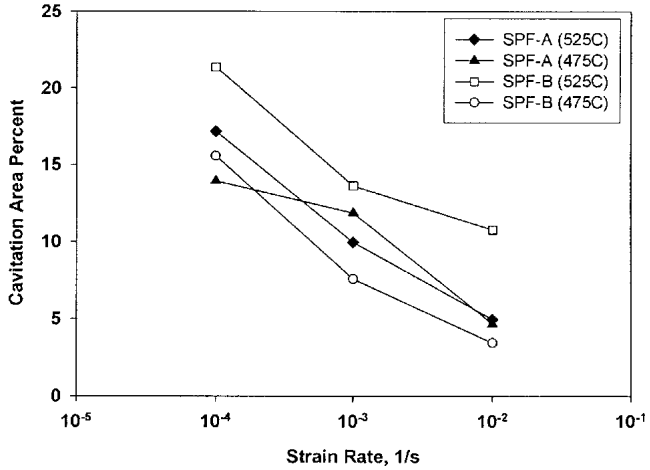

Fig. 12 Average area percentage of cavitation for SPF5083-A and SPF5083-B alloys. Measurements are the average of 1 mm sections over a 25 mm section of the highest strain section of the gauge length.

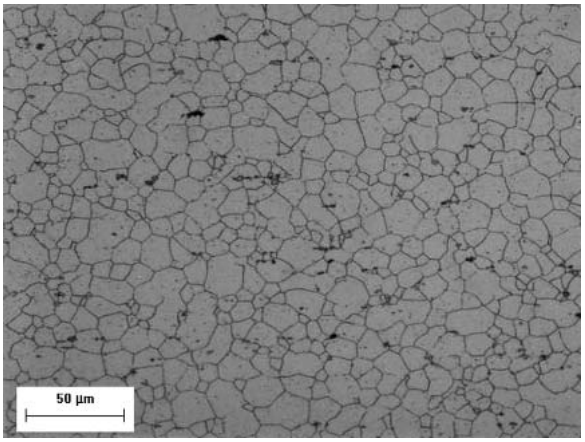

Fig. 13 Micrograph of AA5182-O alloy in the as-received condition

gauge sections from the same two samples are shown in Fig. 14(b) and 15(b). The fraction of cavities is significantly greater in the sample deformed at the slower strain rate. This trend is shown again in Fig. 16, where the gauge section of the AA5182 alloy sample that was deformed at a 1×10^{-4} s^{-1} initial strain rate is shown. It appears that cavities had begun to coalesce, forming very large voids between grains. Failure typically occurs in these alloys once the cavity-weakened material no longer can support the flow stress. This effect of strain rate on the degree of cavitation is a result of the different controlling failure mechanisms in this alloy. At the slower strain rates, the failure is mostly internal cavitation, however, at faster rates this changes to external necking. This is consistent with the *m* value data, which indicate higher rate sensitivity in this alloy at the slower strain rates.

At 475 °C, this alloy showed very poor superplastic response at all strain rates. Optical microscopy of the grip region indicates significant preferential grain growth. As shown in Fig. 17(a), some grains have grown several orders of magnitude larger, while others have remained relatively fine. The fine

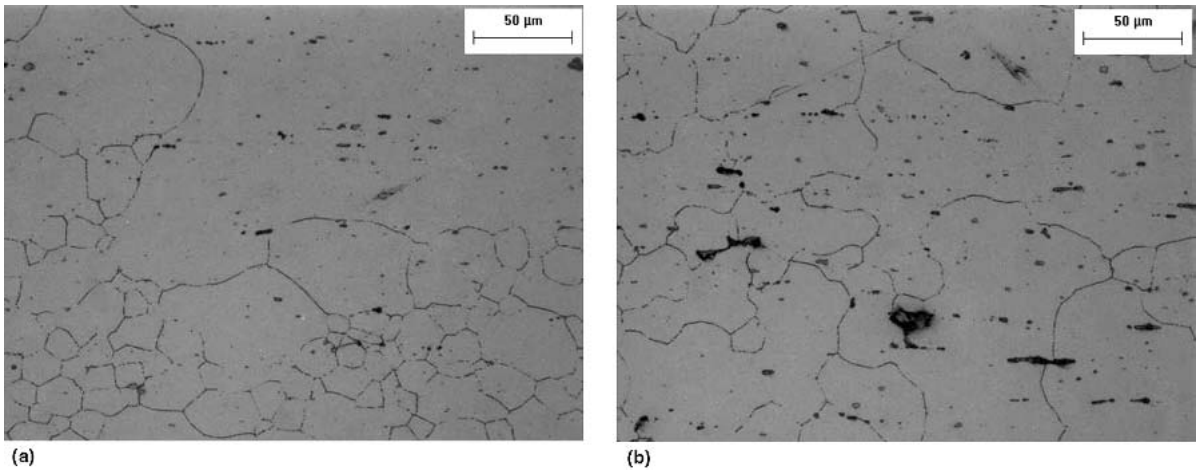

Fig. 14 Micrographs of the (**a**) grip and (**b**) gauge regions of the AA5182 alloy after superplastic deformation at 525 °C and 1×10^{-2} s^{-1} initial strain rate

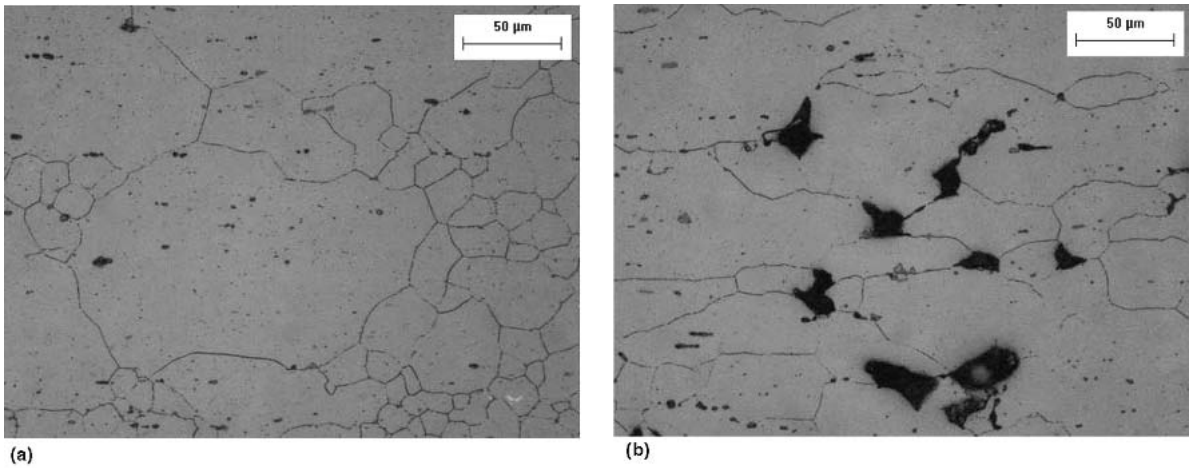

Fig. 15 Micrographs of the (**a**) grip and (**b**) gauge regions of AA5182 alloy after superplastic deformation at 525 °C and a 1×10^{-3} s^{-1} initial strain rate

grains remain in clusters separated by very coarse grains. The poor superplastic response at this temperature is a result of the bimodal grain structure and, subsequently, of the inability of the material to support grain boundary sliding. This abnormal grain growth can probably be attributed to the dissolution of some anchoring precipitates that preferentially allowed some grains to grow quickly while keeping some grains pinned. This has been reported in other Al-Mg alloys and has been linked to Al-Fe intermetallics.[12]

As the test temperature is lowered to 425 °C, the superplastic response significantly improved for all strain rates. As shown in Fig. 17(b), there was very little grain growth in the material at this temperature. This region of deformation may indicate the ideal forming regimen for this alloy where there is significant thermal energy to promote good superplastic response, but not so much that grains begin to grow rapidly.

To further illustrate the difference in deformation and failure mechanisms in this material at the three different strain

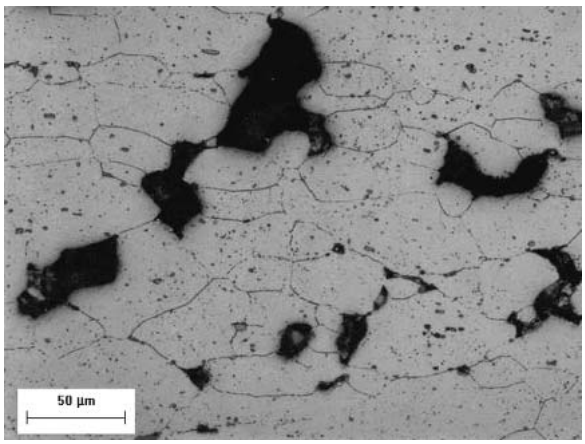

Fig. 16 Micrograph of the gauge region of AA5182 alloy after superplastic deformation at 525 °C and a 1×10^{-4} s^{-1} initial strain rate

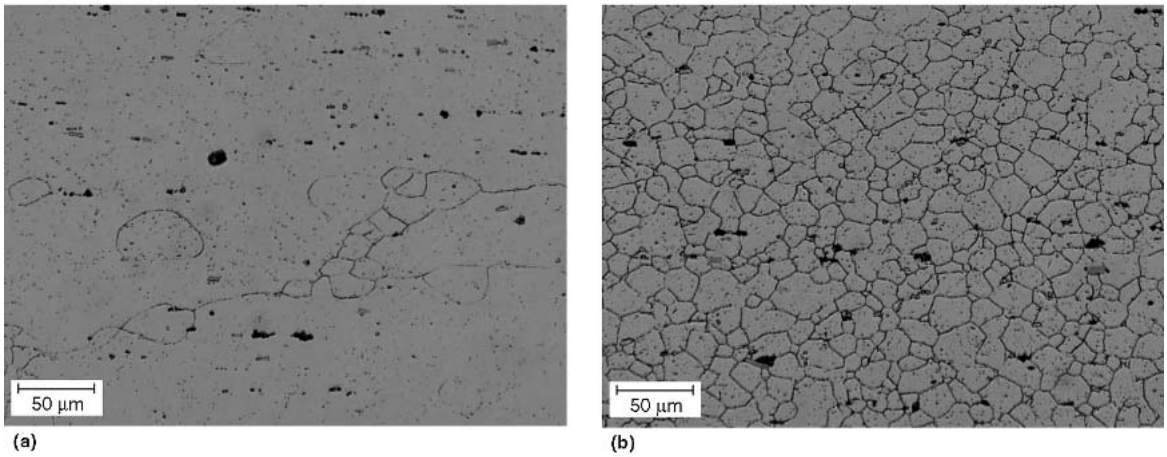

Fig. 17 Micrograph of the grip region of AA5182 alloy after superplastic deformation at a 1×10^{-3} s^{-1} initial strain rate at test temperatures of (**a**) 475 °C and (**b**) 425 °C

rates, micrographs of the failure region are shown in Fig. 18 for samples deformed at 525 °C. It is interesting to note that as the strain rate increases, the specimen experiences more localized necking. This is a result of a change in failure mechanism from internal cavitation at the slower strain rates to a combination of internal cavitation and external necking at the faster strain rate. The sample deformed at the fastest rate appears to have necked down to a point, whereas the other two specimens experienced mostly cavitation with only a small degree of external necking. This is consistent with the notion that at the faster strain rates, these materials experience a loss of *m* value and resistance to necking.

A comparison of the necking behavior in all of the samples tested at 525 °C was performed by measuring the thickness of the material by digital optical microscopy at several locations within the gauge length. Figure 19 shows the percent reduction in thickness for all of the samples tested. The reduction in thickness was measured over a 25 mm span of specimen length. The final measurement was made approximately 2 mm away from the fracture tip. The degree of necking, as quantified in the percentage of thickness reduction, shows that all of the samples showed an increase in external necking behavior with increasing strain rate. The effect of strain rate was found to be significantly more pronounced in the AA5182 alloy specimen, especially between strain rates of 1×10^{-2} s^{-1} and 1×10^{-3} s^{-1}.

5. Discussion

The tests described in this article offer a relatively quick and efficient method of gaining valuable insight into the superplastic responses of Al alloys. Information regarding the effect of strain rate, orientation, and temperature on both total elongation and *m* value can be attained with these tensile tests. The tests are performed under constant CHS conditions, which means that the samples actually experience a decreasing strain rate. At an elongation of 100%, the actual strain rate on the sample is approximately one half of the initial strain rate. While the constant CHS test results in an underestimate of the hardening behavior, it offers a very repeatable method of measuring superplastic response under different test conditions.

The flow behaviors in the two SPF alloys were found to be very similar, with faster strain rates displaying higher flow stresses. However, it appears that the hardening rates (i.e., the increases in flow stress with strain) were significantly greater in the slower strain rate tests for both alloys. This difference in hardening rate is most likely a result of the different mechanisms that control deformation at the three different strain rates. At the slowest rate, the deformation is mostly controlled by diffusional mechanisms at grain boundaries. As the grains grow, the required stresses to continue deformation increase. At faster strain rates, at which the deformation mechanism is a more thermally assisted dislocation motion, the hardening rate is controlled by the dislocation density, which saturates early in the forming cycle.

Alloys such as the AA5xxx series Al that have been processed to have a fine grain size are typically alloyed with elements that form grain boundary-pinning precipitates (or dispersoids). In the test alloys in this study, Mn was used to form Al_6Mn precipitates, which act as grain boundary-pinning agents. The effect of particles such as these on superplastic response and, more specifically, on limiting dynamic grain growth has been investigated.[13,14] While grain growth can limit superplastic response, it has been postulated that maintaining a positive hardening rate $[1/(d\sigma/d\varepsilon)]$, resulting from a low rate of grain growth, can improve overall superplasticity.[15,16]

Total elongation in the SPF alloys was found to be consistently higher for the slowest strain rates. This result seems to contradict the data on *m* value showing a higher *m* value at the middle strain rate. This inconsistency can most likely be explained by the lower flow stresses in the slower test. Al alloys, especially Al-Mg alloys, under superplastic conditions typically fail by cavitation. This process entails the nucleation of voids on grain boundaries, the growth of these voids with strain, and then finally void coalescence.[17] Cavity growth in superplastic deformation is typically controlled by plastic flow, which is driven by the normal stress gradients generated as grains slide past each other.[18] It is possible that samples deformed at the slower rates can withstand a higher cavitation volume due to lower forces on the grain boundaries.

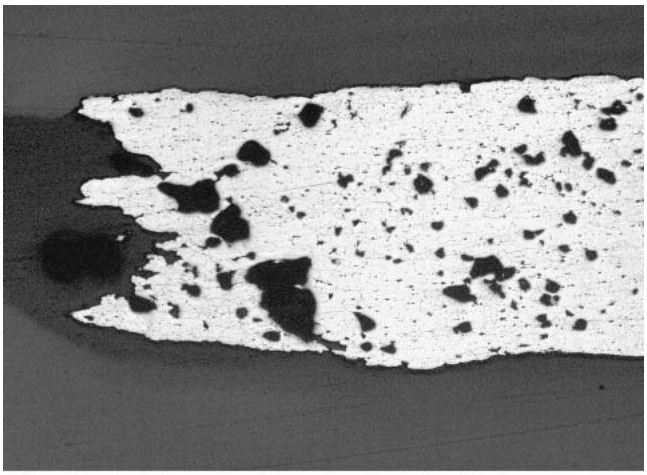

(a)

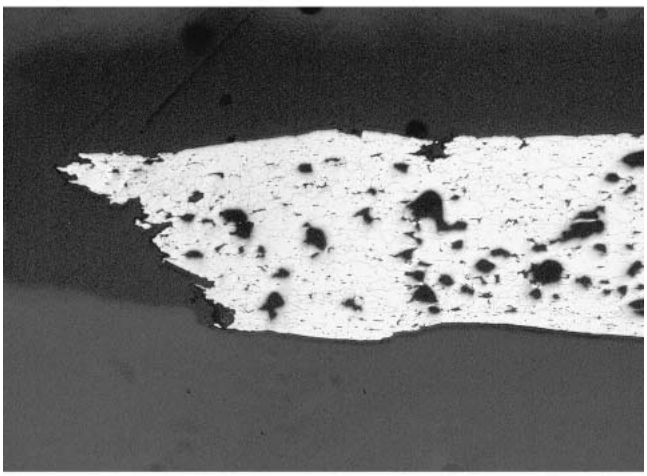

(b)

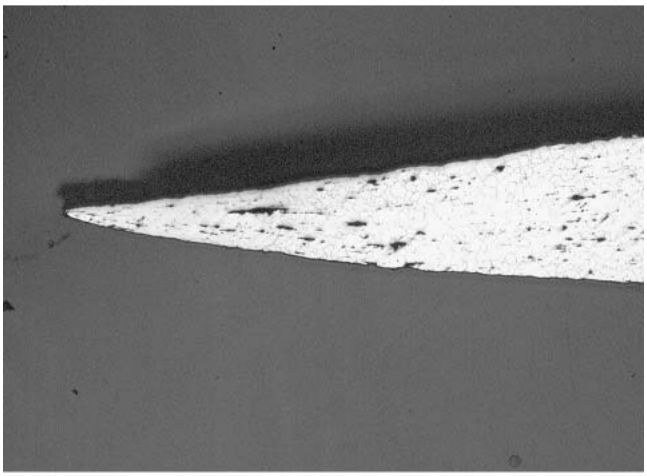

(c)

Fig. 18 Micrographs of the fractured sections of AA5182 alloy after superplastic deformation at initial strain rates of (**a**) 1×10^{-4} s^{-1}, (**b**) 1×10^{-3} s^{-1}, and (**c**) 1×10^{-2} s^{-1}

The results of the tensile tests on the AA5182 alloy help to further illustrate the mechanisms that control superplastic deformation. The total elongations in these tests were significantly lower than those of either of the SPF alloys. This can be attributed to the larger grain size (and hence lower *m* value) and to a lower resistance to grain growth in this alloy. The larger grain size results in a reduced ability to accommodate grain boundary sliding without causing cavities to form. It is interesting to note that total elongation for this conventionally processed alloy had the opposite trend with respect to strain rate than those of the SPF alloys. This can be explained by the lower resistance to grain growth in the AA5182 alloy. As the grains grow faster in the AA5182 alloy compared with the SPF alloys, stress concentrations at grain boundaries increase, creating the required forces to initiate cavitation. These larger grains may be the cause of the significantly higher cavitation rate in the AA5182 alloy sample deformed at the slowest strain rate.

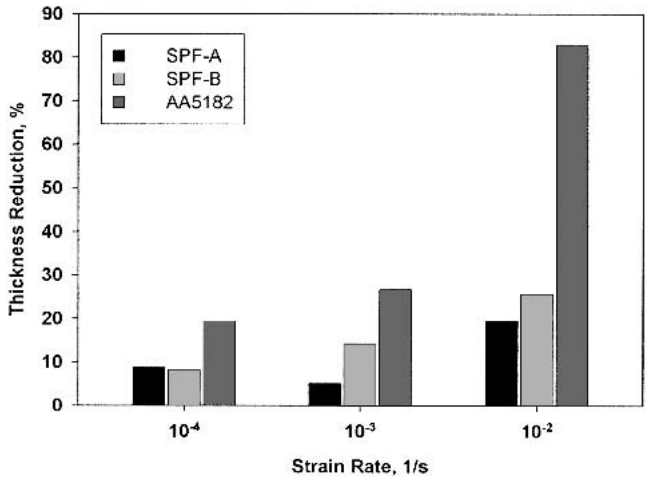

Fig. 19 Percentage reduction in thickness for samples tested at 525 °C based on measurements taken over a 25 mm span of specimen length. The final measurement was made approximately 2 mm away from the fracture.

The effect of temperature is consistent with this notion in that lower temperature tests show slower grain growth and superior superplastic response. The very poor superplastic response at 475 °C for all strain rates was a result of the formation of a bimodal grain structure. This abnormal grain growth may be attributed to the dissolution of certain precipitates in solid solution, which pins grain boundaries and slows grain growth.[12] As the submicron intermetallics (possibly iron-based) begin to dissolve, certain grains are released and grow rapidly, while others remain pinned. At 525 °C, it is possible that all of the intermetallics were in solution producing a relatively homogenous microstructure and, hence, more even grain growth. At temperatures below 425 °C, it appears that there was minimal grain growth, possibly due to these pinning intermetallics.

The controlling deformation mechanism in the AA5182 alloy appears to change from superplasticity to more thermally assisted dislocation motion at faster strain rates. This is evidenced in the change in failure mechanism in the AA5182 alloy from internal cavitation to external necking with increases in strain rate. Total elongation was found to be greatest at the fastest strain rate. Hence, the ideal forming condition for this alloy may not be SPF but rather thermally assisted plastic

deformation. Further work investigating the effect of temperature on the deformation behavior of commercially available, conventionally processed Al-Mg alloys is needed to fully understand their potential.

6. Summary and Conclusions

In this article, a set of tensile tests was presented and was used to characterize the superplastic response of three different aluminum sheet alloys. Two of these alloys were specially processed for superplastic deformation, while the other was conventionally processed. Test results were used in conjunction with optical microscopy to gain information on the effects of strain rate and temperature on superplastic response.

For both alloys specially processed for SPF (SPF5083), total elongation increased with decreases in strain rate. The highest *m* values were found at the middle strain rate, where it is believed the deformation is based on a combination of diffusion-based and thermally assisted dislocation mechanisms. Total elongation and *m* value were found to be higher at the higher temperature of 525 °C for the SPF5083 alloys. Flow stresses were found to be approximately 50-60% higher at the lower temperatures of 475 °C under identical test conditions.

Contrary to the results of the SPF5083 alloy, the AA5182 alloy displayed a significant loss in strain to failure at the slower strain rates and higher temperatures. This can be explained by the lack of grain-pinning mechanisms in the AA5182 alloy, and therefore by the faster grain growth and rate of cavitation, compared with either of the SPF5083 alloys. As evidenced by the change in failure mechanism in the AA5182 alloy from internal cavitation to external necking with increases in strain rate, it appears that the controlling deformation mechanism changes from superplasticity to more thermally assisted dislocation motion at faster strain rates. While the superplastic response of the AA5182 alloy at the lower temperatures and faster strain rates was still found to be significantly lower than those of either of the SPF5083 alloys, these results indicate that it may be possible to use a conventionally processed alloy to superplastically form relatively simple parts in which a relatively fast strain rate can be applied.

References

1. D.H. Avery and W.A. Backofen: "A Structural Basis for Superplasticity," *Trans. ASM*, 1965, *58*(4), pp. 551-62.
2. M.F. Ashby and R.A. Verrall: "Diffusion-Accommodated Flow and Superplasticity," *Acta Metallurgica*, 1973, *21*(2), pp. 149-63.
3. R.C. Gifkins: "Grain-Boundary Sliding and its Accommodation During Creep and Superplasticity," *Metall. Trans.*, 1976, *7A*(8), pp. 1225-32.
4. R.C. Gifkins: "Effect of Grain Size and Stress Upon Grain Boundary Sliding," *Metall. Trans.*, 1977, *8A*(10), pp. 1507-16.
5. H. Iwasaki, K. Higashi, S. Tanimura, T. Komatubara, and S. Hayami: "Superplastic Deformation Characteristics of 5083 Aluminum Alloy" in *Superplasticity in Advanced Materials*, S. Hori, M. Tokizane, and N. Furushiro ed., The Japan Society for Research in Superplasticity, Tokyo, Japan, 1991, pp. 447-52.
6. B.J. Dunwoody, R.J. Stracey, and A.J. Barnes: "Mechanical Properties of 5083 SPF After Superplastic Deformation" in *Superplasticity in Metals, Ceramics and Intermetallics*, *Materials Research Society Symposium Proceedings*, Vol. 196, M.J. Mayo, M. Kobayashi, and J. Wadsworth, ed., Materials Research Society, 1990, pp. 161-66.
7. R.L. Hecht and K. Kannan: "Mechanical Properties of SP 5083 Aluminum After Superplastic Forming" in *Superplasticity and Superplastic Forming*, A. K. Ghosh and T. R. Bieler ed., The Minerals, Metals and Materials Society, Warrendale, PA, 1995, pp. 259-66.
8. H. Imamura and N. Ridley: "Superplastic and Recrystallisation Behaviour of a Commercial Al-Mg Alloy 5083" in *Superplasticity in Advanced Materials*, S. Hori, M. Tokizane, and N. Furushiro ed., The Japan Society for Research in Superplasticity, Tokyo, Japan, 1991, pp. 453-58.
9. J.S. Vetrano, C.A. Lavender, C.H. Hamilton, M.T. Smith, and S.M. Bruemmer: "Superplastic Behavior in a Commercial 5083 Aluminum Alloy," *Scripta Metall.*, 1994, *30*(5), pp. 565-70.
10. R. Verma, P.A. Friedman, and A.K. Ghosh: "Characterization of Superplastic Deformation Behavior of a Fine Grain 5083 Al Alloy Sheet," *Metall. Trans.*, 1996, *27A*(7), pp. 1889-98.
11. P.A. Friedman and A.K. Ghosh: "Control of Superplastic Deformation Rate During Uniaxial Tensile Tests," *Metall. Trans.*, 1996, *27A*(10), pp. 3030-42.
12. B.B. Straumal, W. Gust, L. Dardinier, J.-L. Hoffman, V.G. Sursaeva, and L.S. Shvindlerman: "Abnormal Grain Growth in Al of Different Purity" in *Materials & Design, Symposium J: Light-Weight Materials for Transportation*, Strasbourg, France, 1997, *8*(4-6), pp. 293-95.
13. J.A. Wert: "Grain Refinement and Grain Size Control" in *Superplastic Forming of Structural Alloys*, N.E. Paton and C.H. Hamilton, ed., The Metallurgical Society of AIME, Warrendale, PA, 1982, pp. 69-83.
14. M.J. Stowell: "Design of Superplastic Alloys" in *Deformation of Multi-Phase and Particle-Containing Materials*, *Proc. 4th Riso Int. Symp.*, J.B. Bilde-Sorenson, ed., Roskilde, Denmark, 1983, pp. 119-29.
15. A.K. Ghosh and C.H. Hamilton: "Mechanical Behavior and Hardening Characteristics of a Superplastic Ti-6Al-4V Alloy," *Metall. Trans.*, 1979, *10A*(6), pp. 699-706.
16. A.K. Ghosh: "A New Physical Model for Superplastic Flow" in *Superplasticity Adv. Mater. Mater. Sci. Forum*, T. Langdon, ed., 1994, *170-172*, pp. 39-46.
17. G.H. Edward and M.F. Ashby: "Intergranular Fracture During Power Law Creep," *Acta Metall.*, 1979, *27*(9), pp. 1505-18.
18. J. Pilling and N. Ridley: "Effect of Hydrostatic Pressure on Cavitation in Superplastic Aluminum Alloys," *Acta Metall.*, 1986, *34*(4), pp. 669-79.